

PatchPerPix for Instance Segmentation

Peter Hirsch* Lisa Mais* Dagmar Kainmueller

Berlin Institute of Health / Max Delbrueck Center for Molecular Medicine

{firstname.lastname}@mdc-berlin.de

Abstract

In this paper we present a novel method for proposal free instance segmentation that can handle sophisticated object shapes that span large parts of an image and form dense object clusters with crossovers. Our method is based on predicting dense local shape descriptors, which we assemble to form instances. All instances are assembled simultaneously in one go. To our knowledge, our method is the first non-iterative method that guarantees instances to be composed of learnt shape patches. We evaluate our method on a variety of data domains, where it defines the new state of the art on two challenging benchmarks, namely the ISBI 2012 EM segmentation benchmark, and the BBBC010 C. elegans dataset. We show furthermore that our method performs well also on 3d image data, and can handle even extreme cases of complex shape clusters.

1. Introduction

The task of instance segmentation has a wide range of applications in natural images as well as microscopy images from the biomedical domain. A prevalent class of instance segmentation methods, namely proposal-based methods based on RCNN [9, 10], has proven successful in cases where instance location and size can be well-approximated by bounding boxes. However, in many cases, especially in the biomedical domain, this does not hold: Instances may span widely across the image, and hence multiple instances may have very similar, large bounding boxes. To complicate things, instances may be densely clustered, in some cases overlapping, including crossovers. Proposal-free methods are applicable in such cases, where popular choices include metric learning / instance coloring [15, 4], affinity-based methods [7, 27, 17, 8], and learnt watershed [3, 28]. However, respective pixel-wise predictions do not explicitly capture instance shape, nor are they suitable for disentangling overlapping instances. appearance at different locations of the image [22].

To overcome these limitations, we propose to (1) densely predict representations of the shapes of instance patches, (2) cover the image foreground with the most plausible shape patches, and (3) puzzle together complete instance shapes from these patches by means of partitioning a patch affinity graph. The approach of covering the image by selecting from a redundant set of instance patch predictions allows for naturally handling overlap (including crossovers), as overlapping instance patches can be selected, potentially resulting in pixels covered by multiple instances.

Our general idea is closely related to Singling Out Networks [29]. However, they are different in that they rely on a dictionary of known instances, thereby limiting the variability of objects they can handle, and they only consider predicting whole instances and not patches of instances, thereby limiting the size of feasible object categories.

Our shape prediction network predicts, for each pixel of the input image, a representation of the local shape of the instance this pixel belongs to, namely a shape patch of the pixel’s instance. The architecture we propose, which we term *PatchPerPix*, is derived from the U-Net [23], thus allowing for efficient dense prediction. We achieve predictions of shape representations with hundreds of dimensions by keeping the number of feature maps fixed (instead of reducing) in the upward path of the U-Net. Thus we avoid over-compressing information in the penultimate layer of the U-Net, i.e. we avoid having to predict pixel-wise outputs with hundreds of dimensions from only tens of feature maps.

As representations of instance patch shapes, we explore local binary masks, as well as encodings (i.e. compressed versions) of these. The idea of predicting instance shape masks per pixel of an image has been pursued before [5, 6, 13]. However, all these approaches work on the assumption that a shape mask can capture a complete instance shape. Thus they are designed for object categories common to natural images rather than for disentangling clusters of complex shapes that occupy similar bounding boxes, as relevant in the biomedical domain. Predicting shape encodings instead of binary masks is also not new [13]. However, besides only considering complete

*equal contribution, listed in random order

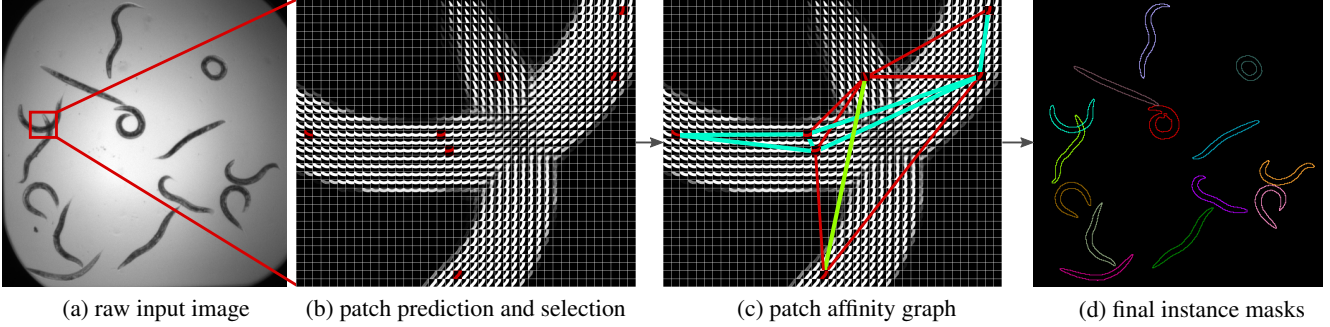


Figure 1: Given the raw input image (a), the neural network predicts dense patches for each pixel which are then used to find a consensus about all pairs of pixels in reach of the patch size. The best patches according to this consensus are selected (b) and connected to form a patch affinity graph. (c) Edges of the patch affinity graph are assigned scores derived from the agreement of the *merged* shape patches with the consensus. The final instance masks are extracted by applying connected component analysis on the positive subgraph. (Edges with negative scores are depicted in red.)

instance shapes as opposed to our patches of instances, in [13], the shape encoding predictor and the decoder are not trained end-to-end, which we show in our work to improve considerably upon separate training.

Concerning the variant of our method that predicts patch shape encodings as shape representations, we propose an architecture that combines a network for predicting a shape encoding with the decoder part of an auto-encoder. Interestingly, our end-to-end architecture has two decoding parts, namely (1) the upward path of the U-Net, which serves for combining high-level image information captured at lower layers with low-level information from upper layers, and (2) the decoder half of an auto-encoder, which is needed to decompress local shape predictions in the end. This opens up the question whether our proposed architecture could not be replaced by a standard encoder-decoder architecture alone, with one encoding and one decoding path, e.g. [2]. Such an architecture takes an image patch the size of our shape patches plus some surrounding receptive field as input, and generates a shape patch for the respective central instance as output. It is applied in a sliding window fashion with stride 1 to generate encodings for each pixel. We investigated this alternative by experimenting with established encoder-decoder architectures in a sliding-window fashion, and found that *using a full U-Net as an encoder*, followed by a standard decoder, considerably outperforms the former.

The variant of our method that predicts local binary masks as shape representations is closely related to methods that employ long-range affinities [14, 27, 17, 8]. In essence, our predicted binary patches can be interpreted as dense affinities in a neighborhood around each pixel. However, in contrast to affinity-based methods, we instead interpret our predictions as patches of instances, from which we puzzle together complete instances. This way, our yielded global instance shapes are guaranteed to be assembled from *learned shape patches*, a property that does

not hold for affinity-based methods. Note that in this respect, our method is related to CELIS [20], which learns to agglomerate super-pixels to form instances with plausible shapes, yet their initial pixel-wise predictions do not capture object shape. Furthermore, our method is related to Flood Filling Networks [11], an iterative method that learns to expand instances one-by-one. In contrast, our method segments all instances simultaneously in one pass.

We show in a quantitative evaluation that our method is the new state of the art on the ISBI 2012 challenge on segmentation of neuronal structures in EM stacks, and it outperforms the previous state of the art [29, 22] on the BBBC010 benchmark microscopy dataset of worms [25] by a large margin. Furthermore, we obtain competitive results to the state of the art method StarDist [24, 26], a specialized proposal-based method for blob-like objects, on 2d and 3d light microscopy images of densely packed cell nuclei. Last but not least, we demonstrate that our method also applies to the complex tree-like shapes of neurons in 3d light microscopy images.

In summary, our contributions are:

- A novel method for segmenting instances of complex shapes that spread widely across an image in crowded scenarios, with overlaps and crossovers. Our method defines the new state of the art on the competitive ISBI 2012 EM segmentation challenge, and vastly outperforms the state of the art on the challenging BBBC010 C. elegans dataset.
- Instance segmentations are guaranteed to be assembled from learnt shape pieces. Our method is, to our knowledge, the first such method that is not iterative, i.e. we compute all instances in one pass.

2. PatchperPix for Instance Segmentation

Our method comprises a CNN to predict dense local shape descriptors, and a one-pass pipeline to assemble all instances simultaneously. The instance assembly pipeline leverages the inherent redundancies in our patch predictions by computing consensus affinities for all pixel pairs. We then rank all patches w.r.t. their agreement with the consensus affinities. Thus, we do not require the prediction of an extra "objectness score" or alike. We select high-ranking patches that fully cover the image foreground by means of a greedy set cover algorithm. Last, we compute affinities between these patches, again based on comparison with the consensus. The final instance segmentation is obtained by partitioning the respective patch affinity graph. Figure 1 provides an overview of our pipeline.

2.1. Learning dense shape descriptors

We use a deep convolutional neural network to predict a fixed-sized patch for each pixel. The size of the patch determines the number of output channel per pixel. The core architecture in our experiments is a U-Net [23]. To enable the high number of outputs, we limit the reduction of feature maps that is commonly performed in the upsampling path.

The size of our patches is a significant hyperparameter. Its choice is a trade-off between a preferably larger patch size and the consequently increased memory footprint. It has to be big enough to handle occlusions and overlaps and capture shape characteristics. What is big enough strongly depends on the data domain. However, larger patches require more feature maps yet the model still has to fit into GPU memory.

In addition to our baseline PatchPerPix model, which we refer to as **ppp**, we developed three extensions: (1) PatchPerPix combined with a separately trained autoencoder (**ppp+ae**), (2) PatchPerPix plus a decoder, trained end-to-end (**ppp+dec**) and (3) an encoder-decoder network to predict the patch of the center pixel directly given the raw input image (**ed-ppp**).

ppp+ae Depending on the application domain, the variety of possible shape patches and the amount of information contained in each patch is limited. Therefore it should be feasible for the network to learn compressed patches. To this end we train a fully convolutional autoencoder on the ground truth binary masks to construct a patch latent space. The main network is modified to output the corresponding latent code vectors instead of the uncompressed patches. This way, with the same number of parameters, we can compute larger patches, or, with a lower number of parameters, patches of the same size. The decoder part of the pretrained autoencoder is used to decompress the encoded vectors.

ppp+dec Here, we attach the decoder part of the autoencoder used in ppp+ae to the end of the U-Net, and train the resulting network end-to-end. As before, the U-Net part of the network outputs the code. To fit end-to-end training onto GPU memory, we sample the codes from a random subset of foreground pixels, which are fed to the decoder network. The loss is back-propagated through both the decoder- and the U-Net part of the network.

ed-ppp Especially when dealing with sparse data, the U-Net performs many dispensable computations, namely on background pixels. Only the patches corresponding to foreground pixels are of use, as background patches do not contain pertinent information. Therefore we build a fully convolutional encoder-decoder network to construct our dense shape descriptors from raw image patches. We use 3×3 down- and upsampling to facilitate the singling out of the center pixel's instance from its neighboring instances. To determine for which pixels to run the encoder-decoder network, we train a slim U-Net to generate a foreground mask in a preceding step.

Algorithm 1 PatchPerPix Algorithm

```

patches, fg_mask  $\leftarrow$  NETWORK_INFERENCE(img)
for all patches  $P_i$  do
  for all pixel pairs  $(i, j)$  in patch  $P_i$  do
     $c1 \leftarrow$  GET_IMAGE_COORDINATE(i)
     $c2 \leftarrow$  GET_IMAGE_COORDINATE(j)
    if
      FG(fg_mask,  $c1$ ) & FG(fg_mask,  $c2$ ) &
      FG(patch,  $i$ ) & FG(patch,  $j$ ) then
        consensus( $c1, c2$ ) += 1
    else if
      FG(fg_mask,  $c1$ ) & FG(fg_mask,  $c2$ ) &
      FG(patch,  $i$ ) & BG(patch,  $j$ ) then
        consensus( $c1, c2$ ) -= 1
    end if
  end for
end for
scores  $\leftarrow$  GET_AGREEMENT(consensus, patches)
SORT_DESCENDING(scores)
patches  $\leftarrow$  SELECT_PATCHES(scores, fg_mask)
PRUNE_COVER(patches)
for all patch pairs  $(k, l)$  in patches do
  patch_affinities( $k, l$ )  $\leftarrow$  consensus( $k, l$ )
end for
 $V \leftarrow$  patches
 $E \leftarrow$  patch_affinities
patchgraph  $\leftarrow$  CREATE_GRAPH( $V, E$ )
instances  $\leftarrow$  PARTITION(patchgraph)

```

2.2. Instance Assembly

In our instance assembly algorithm we consider all foreground patches. For the base model we interpret the center pixel of the predicted patch as a foreground mask, for the other models we learn this mask using one additional output channel. The algorithm consists of 4 steps (see Algorithm 1):

1. Each pair of pixels in the image occurs in multiple patches. For each occurrence we increment or decrement an accumulator that indicates if these pixels belong to the same object or not. For this purpose we consider the patch as binary mask being threshold at a fixed (tunable) parameter. The final value of the accumulator is stored in a consensus map.

2. In a second step we score all patches by their agreement with the consensus. We compute the agreement score as follows: For each foreground-foreground and each foreground-background pixel pair in the patch, we look up the consensus value c in the consensus map. We increment the agreement score of the patch if $c > 0$, and decrement if $c < 0$. We normalize the resulting score by the number of foreground pixels in the respective patch. We rank patches by sorting them by score in descending order.

3. From this ranked list of patches, we iteratively pre-select patches until the foreground mask is fully covered. This pre-selection inadvertently leads to a high oversampling of patches. To speed up the later steps of our pipeline, we prune the pre-selection by a greedy set cover algorithm, i.e. by iteratively selecting the next patch from the pre-selection that covers the most remaining foreground until the whole foreground is covered.

4. In a last step we build a graph from all selected patches. All pairs of patches that overlap are connected by edges. The weight of each edge corresponds to the bilateral affinity consensus between the node patches, computed as follows: For each foreground-foreground pixel pair, where one pixel of the pair stems from one patch and the other pixel from the other patch, we look up the consensus value in the consensus map (if present), and count agreement vs. disagreement as above. This graph is then partitioned to extract the object instances. We partition the graph via connected component analysis, or alternatively by means of the mutex watershed algorithm [27], depending on the application domain.

We implemented the computationally expensive parts of the pipeline with CUDA for efficient execution.

2.3. Overlapping Regions

The case of multiple objects sharing pixels can be found in many biomedical applications, for instance in 2d images of model organisms such as worms or larvae that can crawl on top of each other, or neurons in light microscopy data that share pixels due to the partial volume effect. As pixels

located in areas of overlap belong to multiple instances, their respective shape patch is not well-defined. Hence we exclude these pixels from the entire pipeline.

During training, we achieve this by masking out these areas in the loss computation. To detect overlap at test time, we predict the number of instances per pixel by introducing an additional task for the network, which is trained jointly with the patch predictions. This information is then used in the instance assembly. Pixels in an overlapping region are discarded, their respective shape patches do not contribute to the consensus and cannot be selected. In consequence, this means that (i) only overlapping regions with a maximum diameter of smaller than the size of the patches can be covered completely by patch shapes, and (ii) only occlusions within the range of the neighborhood used in the patch graph generation can be bridged.

3. Experiments

3.1. C. elegans worm disentanglement

The **BBBC010** dataset is a benchmark dataset available from the Broad Bioimage Benchmark Collection [18]¹. It consists of 100 brightfield microscopy images showing multiple *C. elegans* worms per image, which may overlap or cluster. As ground truth, binary masks for foreground/background as well as for each worm separately are provided. As in related work [29, 22], we divide the dataset into a training and testing set with 50 images each, and apply 2-fold cross-validation on the testing set.

Our shape prediction network is a 4-level U-Net [23] starting with 40 feature maps and with two-fold down- and upsampling operations. We do not decrease the number of feature maps during upsampling, such that the representation yielded in the penultimate layer is of similar dimension as the output. In the variant of our method that represents shape patches as binary masks (ppp), we use a patch size of 25×25 . Hence in this case the U-Net has 625 outputs. When predicting shape patches via encodings (ppp+ae and ppp+dec), the U-Net predicts a code of size 252 as intermediate output which is then fed into a decoder network to yield a patch of size 41×41 . We use standard augmentation by transpose, rotate, mirror and elastic deformations. Contrary to [29], we do not augment the number of worms synthetically, but focus on crowded regions during training.

The encoder-decoder network takes the raw image as input and predicts a 41×41 patch as well. It operates on 81×81 input patches, applies 3×3 max-pooling three times and has two convolutional layers on each level. At the bottleneck, the code has an extent of $3 \times 3 \times 256$ and uses 1×1 convolutions. As the network is symmetrical and uses same padding, cropping of the output to obtain the desired

¹BBBC010v1: *C.elegans* infection live/dead image set version 1 provided by Fred Ausubel

patchshape is necessary.

We report results in terms of the AP_{dsb} metric used in the kaggle 2018 data science bowl ($AP_{dsb} = \frac{TP}{TP+FP+FN}$) which takes both missing and spurious instances into account². Furthermore, we also report a range of additional metrics that have been reported by competing approaches, including the slightly different AP_{COCO} , thus enabling direct comparability.

The comparison with state-of-the-art methods [22, 29] and between the variants of our proposed approach are shown in Table 1. The ppp+dec trained end-to-end achieves the best results and improves over competing methods by a margin of more than 15%. Especially for higher IoU thresholds our approach is able to achieve unprecedented performance. Qualitative results are presented in Figure 2.

3.2. Neuron segmentation in electron microscopy

We evaluate our method on the ISBI 2012 EM Segmentation Challenge [1]. Our network architecture as well as the training- and prediction procedure closely follows [27], with the difference that our network has 625 instead of 17 outputs, namely patches of size $1 \times 25 \times 25$, and we do not reduce the number of filters in the upward path of the U-Net.

For consensus voting, here, we weigh each vote by the product of the predicted probabilities at the respective two pixels in a patch. Note that with this variant of PatchPerPix, we obtain a parameter-free method, as no more thresholding of the patch predictions is necessary. For partitioning the patch graph, we use the Mutex-Watershed [27], which avoids false mergers in case of leaky boundaries in the electron microscopy data.

Our method is the leading entry on the Challenge’s leaderboard at present³ among thousands of submissions by more than 200 teams.

3.3. Nuclei segmentation in 2d and 3d

The **dsb2018** dataset was published as part of the kaggle 2018 data science bowl⁴. It features cell and nuclei images recorded under various conditions and different microscopes. To enable better comparison, we use the same subset and train/test split as [24]. The training set consists of 447 and the test set of 50 images. We perform 2-fold cross validation to determine the best number of training iterations of the model as well as the patch threshold.

The architecture is very similar to the model used for the BBBC010 data, with a 4-level U-Net and patch size of 25×25 per pixel (starting with 64 instead of 40 feature maps). Additionally, we regress for each pixel a vector to the center pixel of its instance as an auxiliary task.

²<https://www.kaggle.com/c/data-science-bowl-2018>

³http://brainiac2.mit.edu/isbi_challenge/leaders-board-new

⁴BBBC038v1: available from the Broad Bioimage Benchmark Collection[18]

Moreover, we test our approach on 3d isotropic confocal microscopy images of cell nuclei also used in [26], which we term **nuclei3d**. An example is shown in Figure 3. The dataset consists of 28 recordings and was collected and annotated by [19]. Each 3d volume shows hundreds of nuclei, with multiple dense clusters, and has an average size of $140 \times 140 \times 1100$ pixel. 18 volumes are used for training, 7 for validation, and 3 for testing. We use the same training/validation/test volumes as [26]. Architecture-wise we use a 3-level 3d U-Net, starting with 20 feature maps and tripling the number after each downsampling step. The patch size is $9 \times 9 \times 9$.

Table 2 lists our results in comparison to the previous state of the art [26]. On both the dsb2018 and the nuclei3d dataset, we are en par with the previous state-of-the-art on lower IoU thresholds, and outperform it on higher thresholds. The later is expected, as [26] is based on polyhedral bounding shapes which limits the achievable pixel accuracy.

3.4. Neuron separation in 3d light microscopy data

We aim to identify and segment neurons of the fruit fly brain (GAL4 lines [12]) in an unpublished dataset of 3d multicolor confocal microscopy images. The imaging is done by stochastic labeling able to express different densities of neurons [21]. This task is very challenging as the number of neurons can be high and the samples are captured in such a way as to allow large-scale recording. Moreover, the neurons have a very thin, tree-like structure which may overlap or be intertwined such that their separation is ambiguous.

Similar to nuclei3d, we use a 3-level U-Net with $2 \times$ down- and upsampling and slightly less feature maps. The patch size is $7 \times 7 \times 7$ pixels.

As this dataset is still in the process of being curated and extended, and no competing approach has yet been reported, we do not perform a quantitative evaluation, but show the quality of exemplary results on a test set of two images in Figure 4. This serves as proof-of-concept that our method is applicable and yields reasonable results for thin, complex tree-like structures in 3d image volumes.

4. Conclusion

In this work we present a novel method for instance segmentation of general objects using dense local shape descriptors and a one-pass instance assembly pipeline. The method is able to handle objects of sophisticated shapes that appear in dense clusters with overlaps, including full crossovers. It is the first to assemble all instances from learnt shape patches, simultaneously in one pass. We successfully created models for a range of domains, showing that our method

1. outperforms the state of the art on two challenging

BBBC010					
AP_{COCO}	avAP	$AP_{0.5}$	$AP_{0.75}$	$Recall_{0.8}$	$F1_{0.8}$
Semi-conv Ops [22]	0.569	0.885	0.661	-	-
SON [29]	-	-	-	~ 0.7	-
WormToolbox [25]	-	-	-	-	0.81
ppp+dec (ours)	0.866	0.947	0.899	0.890	0.963

AP_{dsb}	avAP	$AP_{0.5}$	$AP_{0.6}$	$AP_{0.7}$	$AP_{0.8}$	$AP_{0.9}$
ppp	0.718	0.907	0.885	0.827	0.599	0.125
ppp+ae	0.750	0.897	0.873	0.828	0.706	0.257
ppp+dec	0.809	0.937	0.919	0.896	0.792	0.394
ed-ppp	0.731	0.893	0.866	0.838	0.658	0.170

Table 1: Quantitative results for the BBBC010 dataset: Top: We compare our method to existing state-of-the-art approaches in various metrics due to a missing standard. [22] report their results in the COCO evaluation metrics [16], [29] plot the recall for different thresholds and [25] evaluate the percentage of ground truth worms which are matched with a pixelwise F1 score of at least 0.8. Moreover, [22] and [29] input the binary segmentations in addition to the raw brightfield images, thus simplifying the task. Bottom: We show our results for the different architecture setups. ppp+dec trained in an end-to-end fashion is superior.

AP_{dsb}	avAP	$AP_{0.10}$	$AP_{0.20}$	$AP_{0.30}$	$AP_{0.40}$	$AP_{0.50}$	$AP_{0.60}$	$AP_{0.70}$	$AP_{0.80}$	$AP_{0.90}$
dsb2018										
Mask R-CNN[24]	-	-	-	-	-	0.8323	0.7728	0.6838	0.4893	0.1891
StarDist[24]	-	-	-	-	-	0.8641	0.8043	0.6850	0.4495	0.1191
ppp (ours)	0.785	0.919	0.919	0.914	0.901	0.871	0.824	0.752	0.609	0.352
nuclei3d										
IFT-WS[26]	0.446	0.794	0.771	0.708	0.601	0.472	0.364	0.222	0.074	0.005
U-Net+WS[26]	0.595	0.920	0.905	0.872	0.807	0.700	0.593	0.406	0.144	0.005
StarDist 3D[26]	0.628	0.936	0.926	0.905	0.855	0.765	0.647	0.460	0.154	0.004
ppp (ours)	0.640	0.938	0.929	0.905	0.852	0.751	0.655	0.495	0.215	0.020

Table 2: Quantitative results for the nuclei datasets (dsb2018 and nuclei3d): We report average precision (AP_{dsb}) for multiple IoU (intersection over union) thresholds. We are en par with the previous state-of-the-art on lower IoU thresholds, and outperform it on higher thresholds.

benchmark datasets, namely the ISBI 2012 challenge on neuron segmentation in electron microscopy, and the BBBC010 worm dataset,

2. is en par with the state of the art on benchmark data of blob-like shapes, hence showing that our method is generically applicable and performs well also for simple instance shapes, and
3. can be applied to extreme cases of instance shapes, like neurons in 3d light microscopy volumes.

Future work will include semantic object labels in our models. Furthermore, the shape patches predicted by our baseline architecture appear as flattened tensors neglecting

their 2d or 3d spatial nature, which recently has been shown to not fully leverage local structure, with suggested alternatives that we will explore [5].

Acknowledgments

We wish to thank Constantin Pape for his invaluable help in reproducing the network architecture and training- and prediction procedure from [27]. Many thanks also to Carolina Waehlby for her help with the BBBC010 data, and to Stephan Saalfeld and Carsten Rother for very helpful discussions. Moreover, we want to thank the FlyLight Project Team⁵ at Janelia Research Campus for providing the unpub-

⁵<https://www.janelia.org/project-team/flylight>

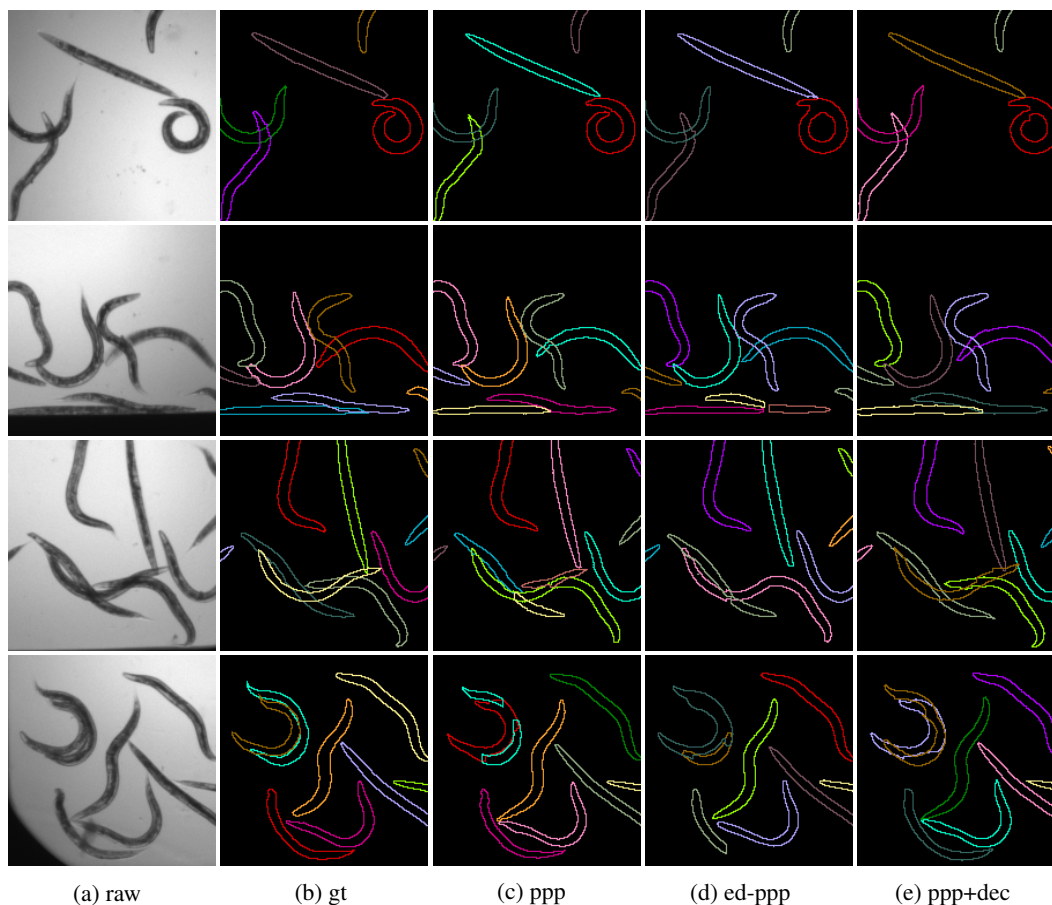


Figure 2: Qualitative results for exemplary challenging regions of the test images. All methods deal well with crowded and overlapping regions, but ppp+dec shows in general less failures. Although ppp may be inferior due to a smaller patch size, which can be seen in a higher number of false splits, it gets difficult shapes such as very bent worms slightly better. In contrast, ed-ppp tends to split instances more often.

lished data and Claire Managan and Ramya Kappagantula (Janelia Project Technical Resources) for their conscientious manual neuron segmentation in fly brain images. P.H., L.M. and D.K. were funded by the Berlin Institute of Health and the Max Delbrueck Center for Molecular Medicine. P.H. was funded by HFSP grant RGP0021/2018-102. P.H., L.M. and D.K. were supported by the HHMI Janelia Visiting Scientist Program. VVD Viewer⁶ is open-source software funded by NIH grant R01-GM098151-01.

References

- [1] Ignacio Arganda-Carreras, Srinivas C Turaga, Daniel R Berger, Dan Cireşan, Alessandro Giusti, Luca M Gambardella, Jürgen Schmidhuber, Dmitry Laptev, Sarvesh Dwivedi, Joachim M Buhmann, et al. Crowdsourcing the creation of image segmentation algorithms for connectomics. *Frontiers in neuroanatomy*, 9:142, 2015. **5**
- [2] Vijay Badrinarayanan, Alex Kendall, and Roberto Cipolla. Segnet: A deep convolutional encoder-decoder architecture for image segmentation. *IEEE transactions on pattern analysis and machine intelligence*, 39(12):2481–2495, 2017. **2**
- [3] Min Bai and Raquel Urtasun. Deep watershed transform for instance segmentation. *CoRR*, abs/1611.08303, 2016. **1**
- [4] Long Chen, Martin Strauch, and Dorit Merhof. Instance segmentation of biomedical images with an object-aware embedding learned with local constraints. In *International Conference on Medical Image Computing and Computer-Assisted Intervention*, pages 451–459. Springer, 2019. **1**
- [5] Xinlei Chen, Ross B. Girshick, Kaiming He, and Piotr Dollár. Tensormask: A foundation for dense object segmentation. *CoRR*, abs/1903.12174, 2019. **1, 6**
- [6] Jifeng Dai, Kaiming He, Yi Li, Shaoqing Ren, and Jian Sun. Instance-sensitive fully convolutional networks. *CoRR*, abs/1603.08678, 2016. **1**
- [7] Jan Funke, Fabian Tschopp, William Grisaitis, Arlo Sheridan, Chandan Singh, Stephan Saalfeld, and Srinivas Turaga. Large scale image segmentation with structured loss based

⁶https://github.com/takashi310/VVD_Viewer

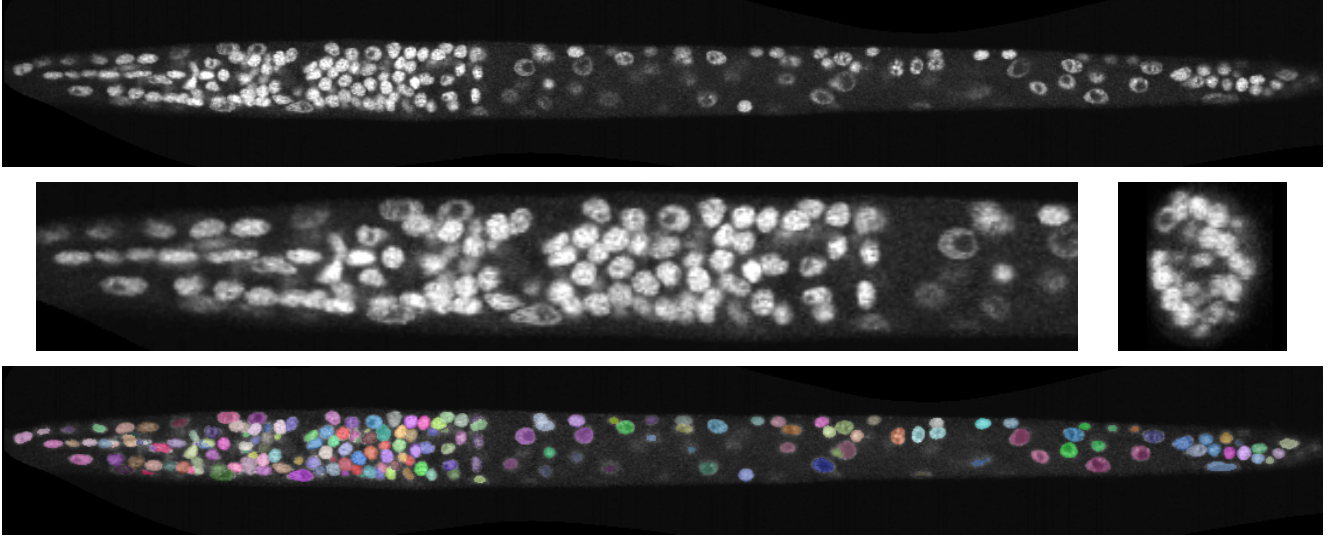


Figure 3: Top: Exemplary xy-slice of a volume in the nuclei3d data set. Densely packed nuclei in the nervous system of the *C. elegans* L1 larva (towards the left) are particularly hard to separate. Center left: Close-up on said nervous system. Center right: Exemplary yz-slice of nervous system. Bottom: Exemplary xy-slice of the segmentation results.

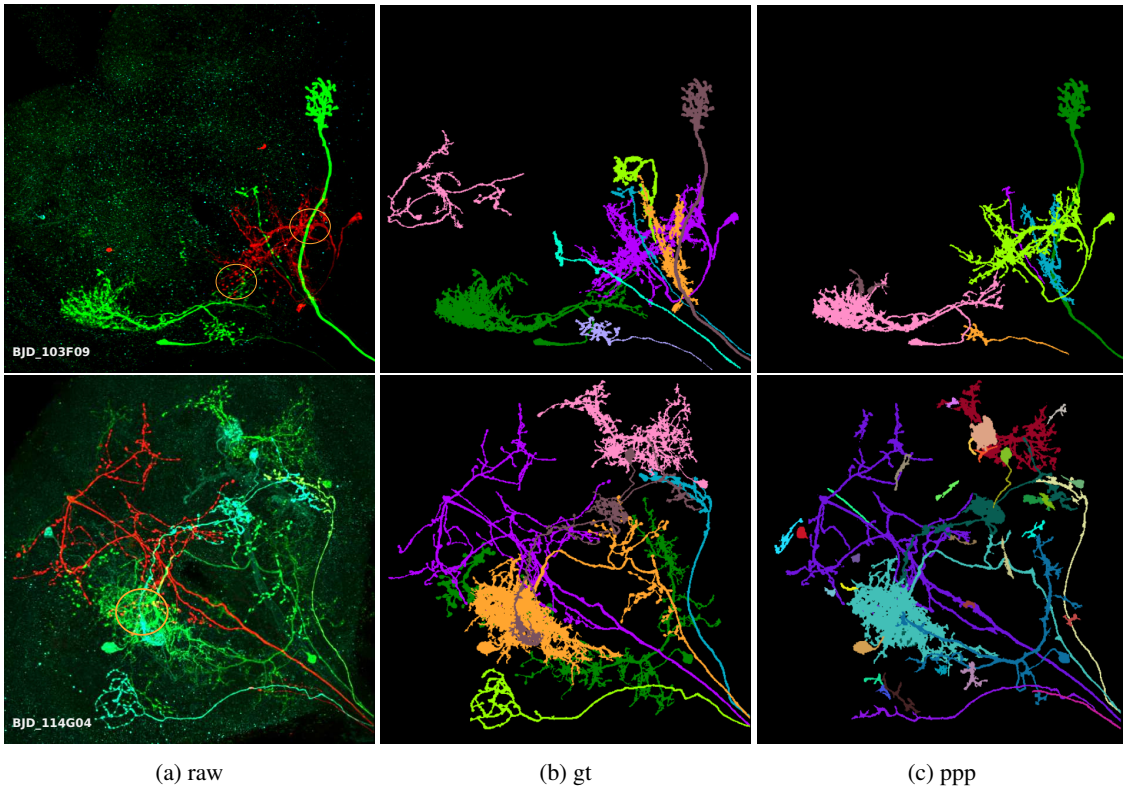


Figure 4: Qualitative results on 3d neuron examples visualized using maximum intensity projection in the z dimension. The orange circles in the raw images (a) indicate actual overlapping areas in 3d. Ground truth data (b) were generated by manual segmentation using VVD Viewer. PatchPerPix (c) shows promising results on this challenging dataset, though future work needs to improve segmentation accuracy in areas with low signal-to-noise ratio.

- deep learning for connectome reconstruction. *IEEE Transactions on Pattern Analysis and Machine Intelligence*, PP:1–1, 05 2018. [1](#)
- [8] Naiyu Gao, Yanhu Shan, Yupei Wang, Xin Zhao, Yanan Yu, Ming Yang, and Kaiqi Huang. Ssap: Single-shot instance segmentation with affinity pyramid. In *Proceedings of the IEEE International Conference on Computer Vision*, pages 642–651, 2019. [1](#), [2](#)
- [9] Ross Girshick, Jeff Donahue, Trevor Darrell, and Jitendra Malik. Rich feature hierarchies for accurate object detection and semantic segmentation. In *Proceedings of the 2014 IEEE Conference on Computer Vision and Pattern Recognition*, CVPR ’14, pages 580–587, Washington, DC, USA, 2014. IEEE Computer Society. [1](#)
- [10] Kaiming He, Georgia Gkioxari, Piotr Dollr, and Ross Girshick. Mask r-cnn, 2017. cite arxiv:1703.06870Comment: open source; appendix on more results. [1](#)
- [11] Michal Januszewski, Jeremy Maitin-Shepard, Peter Li, Jörgen Kornfeld, Winfried Denk, and Viren Jain. Flood-filling networks. *CoRR*, abs/1611.00421, 2016. [2](#)
- [12] Arnim Jenett, Gerald M. Rubin, Teri-T B. Ngo, David Shepherd, Christine Murphy, Heather Dionne, Barret D. Pfeiffer, Amanda Cavallaro, Donald Hall, Jennifer Jeter, Nirmala Iyer, Dona Fetter, Joanna H. Hausenfluck, Hanchuan Peng, Eric T. Trautman, Robert R. Svirskas, Eugene W. Myers, Zbigniew R. Iwinski, Yoshinori Aso, Gina M. DePasquale, Adrienne Enos, Phuson Hulamm, Shing Chun Benny Lam, Hsing-Hsi Li, Todd R. Laverty, Fuhui Long, Lei Qu, Sean D. Murphy, Konrad Rokicki, Todd Safford, Kshiti Shaw, Julie H. Simpson, Allison Sowell, Susana Tae, Yang Yu, and Christopher T. Zugates. A gal4-driver line resource for drosophila neurobiology. *Cell reports*, 2(4):991–1001, Oct 2012. 23063364[pmid]. [5](#)
- [13] Saumya Jetley, Michael Sapienza, Stuart Golodetz, and Philip H. S. Torr. Straight to shapes: Real-time detection of encoded shapes. *CoRR*, abs/1611.07932, 2016. [1](#), [2](#)
- [14] Margret Keuper, Evgeny Levinkov, Nicolas Bonneel, Guillaume Lavoué, Thomas Brox, and Bjorn Andres. Efficient decomposition of image and mesh graphs by lifted multi-cuts. In *Proceedings of the IEEE International Conference on Computer Vision*, pages 1751–1759, 2015. [2](#)
- [15] Kisuk Lee, Ran Lu, Kyle Luther, and H. Sebastian Seung. Learning dense voxel embeddings for 3d neuron reconstruction, 2019. [1](#)
- [16] Tsung-Yi Lin, Michael Maire, Serge Belongie, James Hays, Pietro Perona, Deva Ramanan, Piotr Dollár, and C. Lawrence Zitnick. Microsoft coco: Common objects in context. In David Fleet, Tomas Pajdla, Bernt Schiele, and Tinne Tuytelaars, editors, *Computer Vision – ECCV 2014*, pages 740–755, Cham, 2014. Springer International Publishing. [6](#)
- [17] Yiding Liu, Siyu Yang, Bin Li, Wengang Zhou, Jizheng Xu, Houqiang Li, and Yan Lu. Affinity derivation and graph merge for instance segmentation. *CoRR*, abs/1811.10870, 2018. [1](#), [2](#)
- [18] Vebjorn Ljosa, Katherine L. Sokolnicki, and Anne E. Carpenter. Annotated high-throughput microscopy image sets for validation. *Nature Methods*, 9:637 EP –, Jun 2012. Correspondence. [4](#), [5](#)
- [19] Fuhui Long, Hanchuan Peng, Xiao Liu, Stuart K. Kim, and Eugene Myers. A 3d digital atlas of c. elegans and its application to single-cell analyses. *Nature Methods*, 6(9):667–672, 2009. [5](#)
- [20] Jeremy B Maitin-Shepard, Viren Jain, Michal Januszewski, Peter Li, and Pieter Abbeel. Combinatorial energy learning for image segmentation. In D. D. Lee, M. Sugiyama, U. V. Luxburg, I. Guyon, and R. Garnett, editors, *Advances in Neural Information Processing Systems 29*, pages 1966–1974. Curran Associates, Inc., 2016. [2](#)
- [21] Aljoscha Nern, Barret D. Pfeiffer, and Gerald M. Rubin. Optimized tools for multicolor stochastic labeling reveal diverse stereotyped cell arrangements in the fly visual system. *Proceedings of the National Academy of Sciences*, 112(22):E2967–E2976, 2015. [5](#)
- [22] David Novotny, Samuel Albanie, Diane Larlus, and Andrea Vedaldi. Semi-convolutional operators for instance segmentation. In *The European Conference on Computer Vision (ECCV)*, September 2018. [1](#), [2](#), [4](#), [5](#), [6](#)
- [23] O. Ronneberger, P. Fischer, and T. Brox. U-net: Convolutional networks for biomedical image segmentation. In *Medical Image Computing and Computer-Assisted Intervention (MICCAI)*, volume 9351 of LNCS, pages 234–241. Springer, 2015. (available on arXiv:1505.04597 [cs.CV]). [1](#), [3](#), [4](#)
- [24] Uwe Schmidt, Martin Weigert, Coleman Broadbuss, and Gene Myers. Cell detection with star-convex polygons. *CoRR*, abs/1806.03535, 2018. [2](#), [5](#), [6](#)
- [25] Carolina Wählby, Lee Kamentsky, Zihan H. Liu, Tammy Riklin-Raviv, Annie L. Conery, Eyleen J. O’Rourke, Katherine L. Sokolnicki, Orane Visvikis, Vebjorn Ljosa, Javier E. Irazoqui, Polina Golland, Gary Ruvkun, Frederick M. Ausubel, and Anne E. Carpenter. An image analysis toolbox for high-throughput c. elegans assays. *Nature Methods*, 9(7):714–716, 2012. [2](#), [6](#)
- [26] Martin Weigert, Uwe Schmidt, Robert Haase, Ko Sugawara, and Gene Myers. Star-convex polyhedra for 3d object detection and segmentation in microscopy. *arXiv:1908.03636*, 2019. [2](#), [5](#), [6](#)
- [27] Steffen Wolf, Constantin Pape, Alberto Bailoni, Nasim Rahaman, Anna Kreshuk, Ullrich Köthe, and Fred A. Hamprecht. The mutex watershed: Efficient, parameter-free image partitioning. In *ECCV (4)*, volume 11208 of *Lecture Notes in Computer Science*, pages 571–587. Springer, 2018. [1](#), [2](#), [4](#), [5](#), [6](#)
- [28] Steffen Wolf, Lukas Schott, Ullrich Kothe, and Fred Hamprecht. Learned watershed: End-to-end learning of seeded segmentation. In *Proceedings of the IEEE International Conference on Computer Vision*, pages 2011–2019, 2017. [1](#)
- [29] Victor Yurchenko and Victor S. Lempitsky. Parsing images of overlapping organisms with deep singling-out networks. In *2017 IEEE Conference on Computer Vision and Pattern Recognition, CVPR 2017, Honolulu, HI, USA, July 21-26, 2017*, pages 4752–4760, 2017. [1](#), [2](#), [4](#), [5](#), [6](#)